Single fiber confocal microscope with a two-axis gimbaled MEMS scanner for cellular imaging

Kristen Carlson Maitland

Department of Biomedical Engineering, The University of Texas at Austin, Austin, TX 78712
kmaitland@gmail.com

Hyun Joon Shin

Department of Bioengineering, Rice University, Houston, TX 77251
Korea Institute of Science and Technology, Seoul, 136-791 Korea
hyunj.shin@gmail.com

Hyejun Ra, Daesung Lee, and Olav Solgaard

Department of Electrical Engineering, Stanford University, Stanford, CA 945305
hra@stanford.edu daesung@stanford.edu solgaard@stanford.edu

Rebecca Richards-Kortum

Department of Bioengineering, Rice University, Houston, TX 77251
rkortum@rice.edu

Abstract: We present a single fiber reflectance confocal microscope with a two dimensional MEMS gimbaled scanner. Achieved lateral and axial resolutions are 0.82 μm and 13 μm, respectively. The field of view is 140 x 100 μm at 8 frames/second. Images and videos of cell phantoms and tissue are presented with sub-cellular resolution.

OCIS codes: (110.2350) Imaging systems: Fiber optics imaging; (170.1790) Medical optics and biotechnology: Confocal microscopy; (170.5810) Medical optics and biotechnology: Scanning microscopy

References and links

1. T. Wilson, *Confocal Microscopy*, (Academic Press, San Diego, Calif., 1990).
2. T. Collier, A. Lacy, R. Richards-Kortum, A. Malpica, and M. Follen, "Near real-time confocal microscopy of amelanotic tissue: detection of dysplasia in ex vivo cervical tissue," Acad. Radiol. **9,** 504-512 (2002).
3. K. D. Carlson, I. Pavlova, T. Collier, M. Descour, M. Follen, and R. Richards-Kortum, "Confocal microscopy: Imaging cervical precancerous lesions," Gynecol. Oncol. **99,** S84-S88 (2005).
4. A. F. Gmitro and D. Aziz, "Confocal microscopy through a fiber-optic imaging bundle," Opt. Lett. **18,** 565-567 (1993).
5. C. P. Lin and R. H. Webb, "Fiber-coupled multiplexed confocal microscope," Opt. Lett. **25,** 954-956 (2000).
6. K. B. Sung, R. Richards-Kortum, M. Follen, A. Malpica, C. Liang, and M. Descour, "Fiber optic confocal reflectance microscopy: a new real-time technique to view nuclear morphology in cervical squamous epithelium in vivo," Opt. Express **11,** 3171-3181 (2003).
7. C. Boudoux, S. H. Yun, W. Y. Oh, W. M. White, N. V. Iftimia, M. Shishkov, B. E. Bouma, and G. J. Tearney, "Rapid wavelength-swept spectrally encoded confocal microscopy," Opt. Express **13,** 8214-8221 (2005).
8. D. L. Dickensheets and G. S. Kino, "Micromachined scanning confocal optical microscope," Opt. Lett. **21,** 764-766 (1996).
9. W. Piyawattanametha, H. Toshiyoshi, J. LaCosse, and M. C. Wu. "Surface-micromachined confocal scanning optical microscope," in *Conference on Lasers and Electro-Optics* (Optical Society of America, San Francisco, CA, 2000), pp. 447-448.
10. M. O. Freeman. "Miniature high-fidelity displays using a biaxial MEMS scanning mirror," in *SPIE MOEMS Display and Imaging Systems* (SPIE, San Jose, CA, 2003), pp. 56-62.
11. M. Kozhevnikov, R. Ryf, D. T. Neilson, P. Kolodner, C. A. Bolle, A. R. Papazian, J. Kim, and J. V. Gates, "Micromechanical optical crossconnect with 4-F relay imaging optics," IEEE Photonics Technol. Lett. **16,** 275-277 (2004).

#72437 - $15.00 USD Received 28 June 2006; revised 30 August 2006; accepted 31 August 2006

12. P. M. Hagelin, U. Krishnamoorthy, J. P. Heritage, and O. Solgaard, "Scalable optical cross-connect switch using micromachined mirrors," IEEE Photonics Technol. Lett. **12,** 882-885 (2000).
13. S. Kwon, V. Milanovic, and L. P. Lee, "Vertical combdrive based 2-D gimbaled micromirrors with large static rotation by backside island isolation," IEEE J Quantum Electron. **10,** 498-504 (2004).
14. D. Lee and O. Solgaard. "Two-axis gimbaled microscanner in double SOI layers actuated by self-aligned vertical electrostatic combdrive," in *Solid-State Sensor, Actuator and Microsystems Workshop*, Hilton Head Island, (2004), pp. 352-355.
15. D. L. Dickensheets and G. S. Kino, "Silicon-micromachined scanning confocal optical microscope," J MEMS **7,** 38-47 (1998).
16. Y. Shao and D. L. Dickensheets. "MEMS three-dimensional scan mirror," in *SPIE MOEMS Display and Imaging Systems II* (SPIE, San Jose, CA, 2004), pp. 175-183.
17. H. Ra, Y. Taguchi, D. Lee, W. Piyawattanametha, and O. Solgaard. "Two-dimensional MEMS scanner for dual-axes confocal in vivo microscopy," in *Tech. Digest of IEEE International Conference on MEMS*, (IEEE, Turkey, 2006), pp. 862-865.
18. T. D. Wang, M. J. Mandella, C. H. Contag, and G. S. Kino, "Dual-axis confocal microscope for high-resolution in vivo imaging," Opt. Lett. **28,** 414-416 (2003).
19. T. Xie, H. Xie, G. K. Fedder, and Y. Pan, "Endoscopic optical coherence tomography with a modified microelectromechanical systems mirror for detection of bladder cancers," Appl. Opt. **42,** 6422-6426 (2003).
20. H. Xie, Y. Pan, and G. K. Fedder, "Endoscopic optical coherence tomographic imaging with a CMOS-MEMS micromirror," Sensor Actuat. A-Phys. **103,** 237-241 (2003).
21. S. Kwon and L. P. Lee, "Micromachined transmissive scanning confocal microscope," Opt. Lett. **29,** 706-708 (2004).
22. T. Dabbs and M. Glass, "Fiber-optic confocal microscope: FOCON," Appl. Opt. **31,** 3030-3035 (1992).
23. T. Wilson and A. R. Carlini, "Size of the detector in confocal imaging systems," Opt. Lett. **12,** 227-229 (1987).
24. M. Gu, C. J. R. Sheppard, and X. Gan, "Image formation in a fiber-optical confocal scanning microscope," J Opt. Soc. Am. A **8,** 1755-1761 (1991).
25. K. Sokolov, J. Galvan, A. Myakov, A. Lacy, R. Lotan, and R. Richards-Kortum, "Realistic three-dimensional epithelial tissue phantoms for biomedical optics," J Biomed. Opt. **7,** 148-156 (2002).
26. Squier and Wertz, "Structure and Function of Oral Mucosa," in *Oral Mucosal Drug Delivery*, M. Rathbone, ed. (Marcel Dekker, Inc., New York, 1996).
27. C. J. Balas, G. C. Themelis, E. P. Prokopakis, I. Orfanudaki, E. Koumantakis, and E. S. Helidonis, "In vivo detection and staging of epithelial dysplasias and malignancies based on the quantitative assessment of acetic acid-tissue interaction kinetics," J Photochem. Photobiol. B **53,** 153-157 (1999).
28. R. Drezek, T. Collier, C. Brookner, A. Malpica, R. Lotan, and R. Richards-Kortum, "Laser scanning confocal microscopy of cervical tissue before and after application of acetic acid," AM J Obstet. Gynecol**.,** 1135-1139 (2000).
29. C. Liang, K.B. Sung, R. Richards-Kortum, and M. Descour, "Design of a high-numerical-aperture miniature microscope objective for an endoscopic fiber confocal microscope," Appl. Opt. **41**, 4603-4610 (2002)
30. M. Chidley, K. Carlson, R. Richards-Kortum, and M. Descour, "Design, assembly, and optical bench testing of a high-numerical-aperture miniature injection-molded objective for fiber-optic confocal reflectance microscopy," Appl. Opt. **45**, 2545-2554 (2006).

1. Introduction

Confocal microscopy is an established optical imaging technique used to obtain high-resolution images of cells [1]. This point scanning technique uses a pinhole to reject out of focus light to improve lateral resolution and provide optical sectioning. The optical sectioning capability of confocal microscopy allows depth resolution in bulk tissue. Confocal reflectance microscopy has been demonstrated to have significant potential to detect sub-cellular morphologic changes and alterations in tissue architecture associated with the earliest stages of cancer [2, 3]. Translation of this technology for *in vivo* application using optical fibers and miniature optics will provide clinicians a real-time view of cellular structure, without removal of tissue.

In addition to miniaturization of optics, a major hurdle for *in vivo* imaging is accomplishing fast image acquisition. Many techniques have been explored using optical fibers; in general, they can be broken down into two groups: multi-fiber and single fiber systems. Beam scanning across a fiber bundle allows the scanning mechanism to be placed at the proximal end of the optical fibers, where size is unconstrained. Both coherent [4] and incoherent [5] optical fiber bundles have been used for *en face* image formation. *In vivo* imaging of the cervix has been presented using a coherent fiber bundle and a miniature objective lens [6]. Single fiber confocal microscopes, using individual optical fibers for illumination and detection, can employ one of many beam scanning or object scanning

#72437 - $15.00 USD Received 28 June 2006; revised 30 August 2006; accepted 31 August 2006

techniques to construct an image. Two that are most practical for *in vivo* endoscopic imaging include spectrally-encoding the fast axis [7] and using micromirrors to scan the beam after exiting the fiber [8, 9].

Microelectromechanical systems (MEMS) have enabled the miniaturization of scanning mirrors for placement at the distal end of fiber-based scanning microendoscopes. Other applications for beam-scanning micromirrors include displays and fiber switches [10-12]. Decoupled two-axis scanning has been demonstrated using vertical combdrives in polysilicon and Silicon-on-Insulator (SOI) [13, 14]. SOI technology is attractive for fabrication of MEMS mirrors due to features such as flat mirror surface and relatively simple fabrication.

A miniature scanning confocal microscope using two single-axis micromirrors was proposed and demonstrated by Dickensheets and Kino [15]. This compact module achieved high resolution confocal imaging at 20 frames/second over a 90 μm × 90 μm field of view with a 1.1 mm working distance and 0.25 numerical aperture. More recent advances in scanning technology for confocal microscopy include three-dimensional scanning deformable micromirrors [16] and micromirrors for dual-axes confocal microscopy [17, 18]. In addition to confocal microscopy, MEMS mirrors have also been used for endoscopic optical coherence tomography (OCT). *Ex vivo* OCT imaging of rat bladder has been accomplished using a single-axis MEMS mirror [19, 20]. MEMS scanning confocal microscopes have also been fabricated using electrostatically actuated microlenses for focusing and scanning [21].

Many technologies have been explored to miniaturize confocal microscopes. High deflection MEMS scanners can provide fast scanning and high resolution imaging, using appropriate lens systems, in a compact package. In this paper, we present a single fiber confocal microscope (SFCM) with post-fiber beam scanning by a two-dimensional (2D) electrostatic comb-drive gimbaled MEMS scanner [14] with high resolution. 2D microscanners are more complicated to fabricate than single axis microscanners; however, the design and alignment of high resolution optics, especially in a miniature system, are much easier with a 2D microscanner than with two 1D microscanners. We have achieved image acquisition at 8 frames/second with a field of view of 140 μm × 100 μm with a 3.3 mm working distance and 0.32 numerical aperture. Lateral and axial resolutions are measured at 0.82 μm and 13 μm, respectively.

2. Materials and methods

2.1 Optical system

The confocal microscope illustrated in Fig. 1 uses a single mode fiber for the illumination and detection pinhole. The 635 nm laser diode (LD) light source is fiber coupled to a single-mode (SM), polarization-maintaining (PM) optical fiber. Polarizing beamsplitters (PBS) and a quarter-wave (λ/4) plate were inserted into the optical system to minimize interference due to reflections at fiber surfaces. The illumination light exiting the fiber is collimated to a beam diameter of 0.5 mm, matched to the micromirror diameter. In order to maximize the beam size reflected off the mirror, the angles of incident and reflected light are minimized to approximately 11 degrees, which is only limited by the size of the optics mounts used for the collimator and the first lens of the telescope. The gimbaled micromirror scans the beam in the horizontal direction at the resonance frequency of the inner axis of the mirror, and in the vertical direction at a low frequency using the outer axis. A Keplerian telescope is used to form an image of the micromirror in the entrance aperture of the objective lens to achieve telecentricity. These two lenses are selected to magnify the beam size and improve resolution without significantly compromising scan angle and field of view. A water immersion microscope objective lens (Olympus 40×, 0.8 NA, 3.3 mm working distance) focuses the scanned beam into the sample. Backscattered light is recollected and focused into the SM/PM fiber by the same optical system and passed to an avalanche photodiode (APD) detector through a multi-mode (MM) fiber. The detector and electronics controlling the scanning of the micromirror are coupled to a frame grabber, allowing real-time viewing and recording of images.

#72437 - $15.00 USD Received 28 June 2006; revised 30 August 2006; accepted 31 August 2006

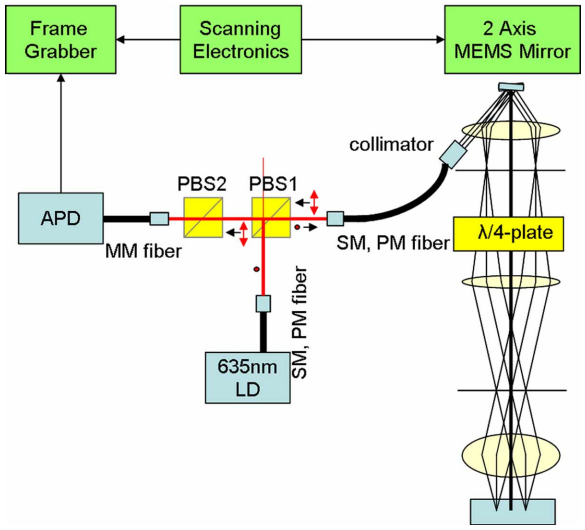

Fig. 1. Schematic of SFCM with microscanner. LD, laser diode; SM, single-mode; PM, polarization-maintaining; MM, multi-mode; PBS, polarizing beam splitter; APD, avalanche photo-diode.

2.2 Microscanner

The MEMS scanner employed in the single fiber confocal microscope has a significant impact on image quality. The scanner used in the SFCM and pictured in Fig. 2 is a 2D gimbaled scanner actuated by vertical, electrostatic combdrive actuators [14]. The scanner is fabricated by performing four steps of deep-reactive ion etching (DRIE) on a double SOI wafer. The mirror size is 500 μm × 500 μm. The inner axis of the mirror is controlled with a voltage signal, $V = V_{DC} + V_{AC} \sin \varpi t$, at the resonance frequency of the mirror, 6.95 kHz, and DC and AC voltage levels of 29 and 9 V, respectively. The corresponding optical deflection is measured to be approximately +/- 4 degrees. The outer axis is actuated with a low frequency sawtooth wave at 8 Hz, with a voltage scan from 0 – 150 V, yielding a measured optical deflection of 6 degrees. These scan ranges, along with the mirror diameter, *D*, and wavelength, λ, can be used to calculate the maximum number of resolvable spots, *N*. Using the Rayleigh criterion for resolution, $N \cong \frac{\theta_{\max}}{\delta\theta} \cong \frac{\theta_{\max} D}{\lambda}$, where $\theta_{\max}$ is the total optical scan range and $\delta\theta$ is the divergence angle, the total number of resolvable spots for our microscanner driven with the described waveforms and illuminated with 850 nm light is approximately 110×82.

#72437 - $15.00 USD Received 28 June 2006; revised 30 August 2006; accepted 31 August 2006

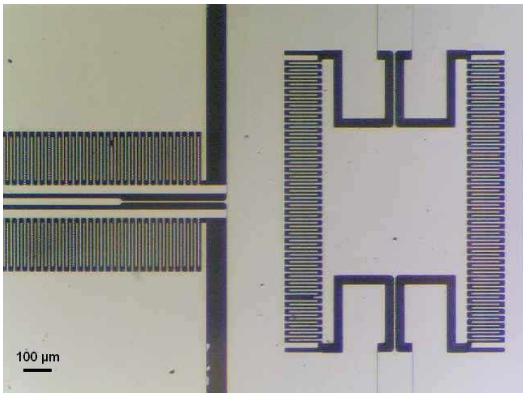

Fig. 2. Optical image of microscanner showing 500 µm x 500 µm active area of mirror and comb teeth to drive scanning in the horizontal and vertical directions. Scale bar 100 µm.

2.3 Resolution

The use of a single mode fiber as the illumination and detection pinholes achieves confocal operation with a micron-scale pinhole [22]. Due to underfilling of the objective lens, the effective NA is approximately 0.32. The beam could be expanded to fill more of the back aperture of the objective lens; however, an increase in beam size reduces the scanning angle. Effectively, either NA and axial resolution or scanning angle and field of view can be improved with a deterioration of the other. This tradeoff can be optimized for the specific imaging application.

Using the fiber NA of 0.12, the 1.5 µm fiber spot size radius as the detection pinhole, and $v = \frac{2\pi}{\lambda} r NA_{fiber}$, the normalized pinhole radius v_p can be calculated as 1.78. The normalized half-width $v_{1/2}$ of an image of a point object is determined to be approximately 1.26 from the plot of the of $v_{1/2}$ as a function of detector size v_p in [23]. Using $r_{FWHM} = \frac{v_{1/2}\lambda}{\pi NA_{objective}}$, the lateral resolution is calculated to be 0.80 µm for the center of the field of view.

Axial resolution is also determined by using the optical fiber as a pinhole detector. The mirror active area and telescope magnification have a significant effect on the NA, which can limit the axial resolution. For 635 nm wavelength, fiber NA of 0.12 and spot size radius of 1.5 µm, Gu's dimensionless fiber spot parameter $A = \left(\frac{2\pi NA r_0}{\lambda} \right)^2$ [24], is calculated to be 3.17 for this configuration of the SFCM. The half-width $u_{1/2}$ of the PSF intensity plot $I(u)$ is measured to be 3.67 optical units for A = 3.17 [24]. Using $z_{FWHM} = \frac{u_{1/2}\lambda}{4\pi n \left(\sin \frac{\alpha}{2} \right)^2}$ and an effective NA of 0.32, the full-width half-maximum (FWHM) axial resolution can be calculated as 9.50 µm.

2.4 Tissue samples

A tissue phantom [25] containing multiple layers of SiHa cervical epithelial cancer cells in collagen was used to demonstrate the cellular imaging capability of the SFCM in dense biological tissue. The tissue phantom was prepared by resuspending cultured SiHa cells in

#72437 - $15.00 USD Received 28 June 2006; revised 30 August 2006; accepted 31 August 2006

buffered collagen type I. Imaging was performed after the cells were allowed to grow for 24 hours into a dense structure similar to epithelial tissue.

To progress to the next level of biological complexity, *ex vivo* tissue samples of porcine oral mucosa were imaged. The anatomy of porcine oral mucosa makes this an attractive animal model for studies of human oral cancer development. Porcine oral mucosa is characterized by a moderately keratinized, squamous mucosa similar to human oral mucosa, unlike many of the typical small laboratory animals, such as rats, hamsters, and guinea pigs, which have highly keratinized oral epithelium [26]. Fresh pig oral tissue was obtained from a slaughter house for SFCM imaging. Before imaging, white vinegar was applied to the tissue to increase nuclear contrast in confocal imaging. Acetic acid, a major constituent of vinegar, has been previously demonstrated to increase scattering from nuclei in reflectance confocal imaging [27, 28].

2.5 Image processing

The raw images are distorted or stretched at the edges of the frame in both the horizontal and vertical directions due to the sinusoidal driving signal in the horizontal direction and the non-linear scanning of the electrostatic combdrive actuators in 2D. Effectively, the speed of the scanner at the edge of the frame is slower than at the center. Most of this distortion is removed by resampling the pixels to compensate for the non-linear scan.

3. Results

3.1 Measured resolution and field of view

A United States Air Force (USAF) resolution test target was used to measure the lateral and axial resolutions and the field of view (FOV) of the SFCM. Figure 3 shows an SFCM video of the 7th group of the USAF resolution test target. The smallest element in the 7th group has a line spacing of 228 line pairs/mm, corresponding to a line width of approximately 2.2 μm. Using the 10% to 90% edge response (Fig. 4) from an unsaturated image of the USAF resolution test target, the lateral resolution was measured as 0.82 μm. This experimental value corresponds well to our calculated FWHM value of 0.80 μm.

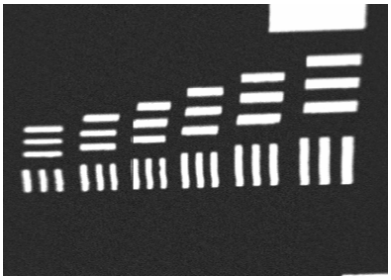

Fig. 3. (798 KB) Video obtained at 8 frames/second of USAF resolution test target translated laterally in object plane of SFCM. The smallest elements in this frame (USAF Group 7 Element 6) are 2.2 μm in width. Field of view is 140 μm x 100 μm.

#72437 - $15.00 USD Received 28 June 2006; revised 30 August 2006; accepted 31 August 2006

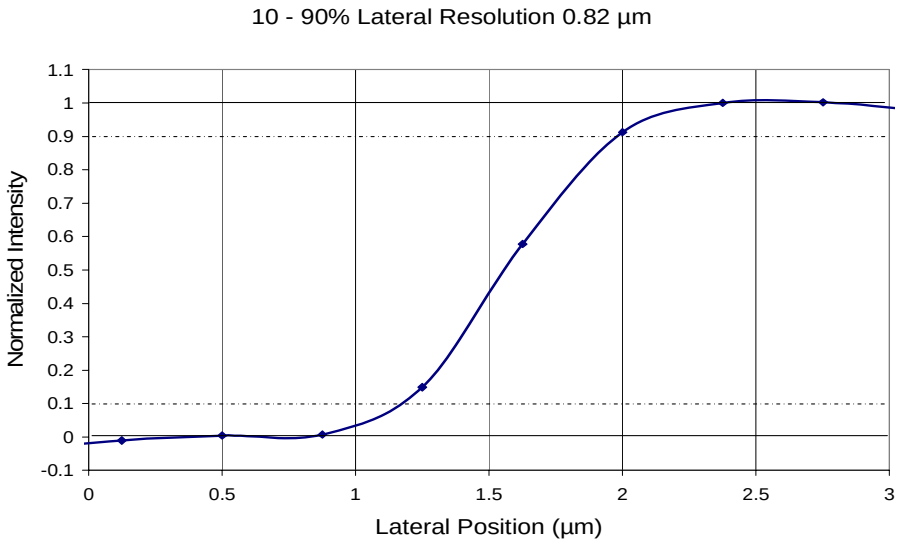

Fig. 4. Line profile or intensity distribution of an edge of a Group 7 Element 2 edge taken from an unsaturated image of a USAF resolution test target. The 10-90% rise distance is measured to be 0.82 µm.

The axial response was measured by moving a reflective surface through the focal plane of the SFCM. Detected signal was measured and plotted (Fig. 5) versus axial position for 0.5 µm increments in the axial position. The full-width half-maximum axial resolution is 13 µm, which is slightly worse than our theoretical axial resolution calculation of 9.5 µm. This small difference may be attributed to slight misalignment within the system.

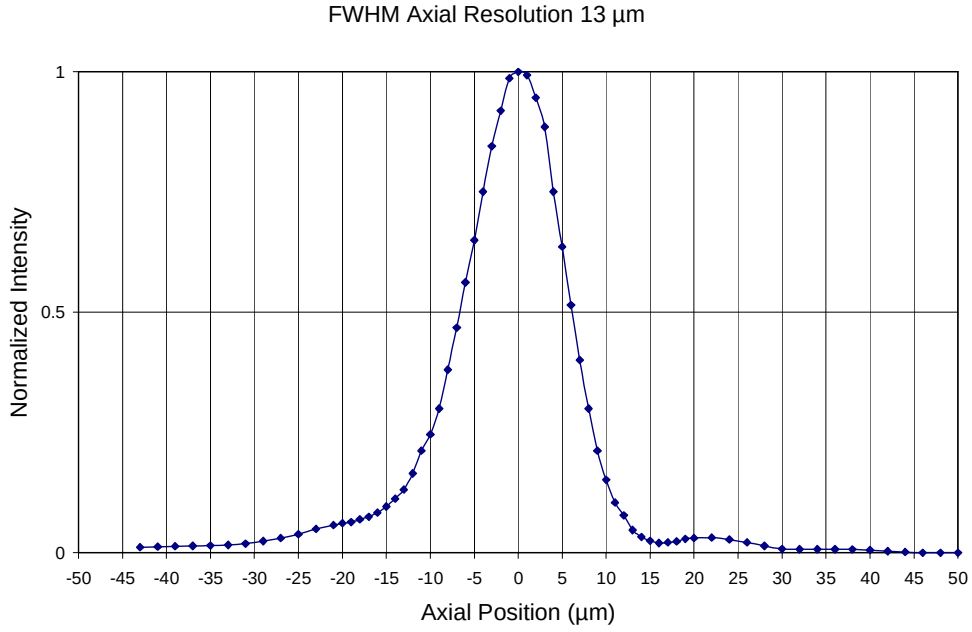

Fig. 5. Normalized signal as a function of axial position, resulting in a SFCM FWHM axial resolution of 13 µm.

#72437 - $15.00 USD Received 28 June 2006; revised 30 August 2006; accepted 31 August 2006

The field of view was measured by lateral translation of an object across the image. The inner axis of the mirror scanning at its resonance frequency produced an image width of 140 µm. The mirror's outer axis, scanning at a frequency significantly below its resonance frequency, produced an image height of 100 µm.

3.2 Cellular imaging

Tissue phantoms made of SiHa cervical cells and collagen were imaged with a commercially available reflectance confocal microscope (Lucid Vivascope) and the SFCM. The Lucid Vivascope uses 830 nm illumination and has a measured axial resolution of 3 µm. Figure 6 presents (a) an image obtained with the Lucid Vivascope and (b) a video obtained with the SFCM. The 500 µm x 500 µm Lucid image includes a frame demonstrating the relative size of the 140 µm x 100 µm SFCM image. Images from both confocal microscopes show single cell layers.

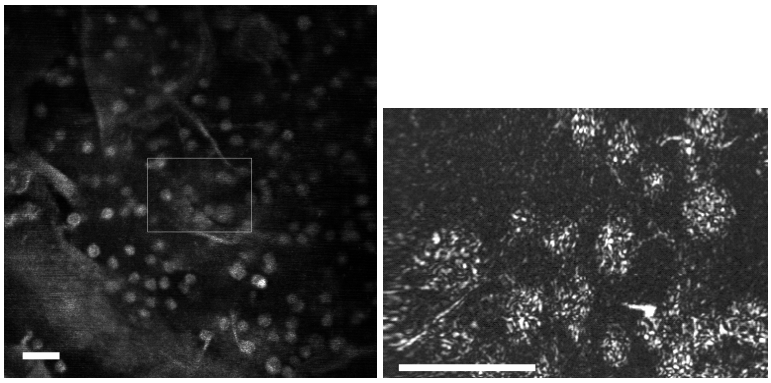

(a) (b)

Fig. 6. Tissue phantom containing SiHa cervical cancer cells and collagen. (a) Image obtained using a commercial reflectance confocal microscope at 830 nm. Field of view: 500 µm x 500 µm. (b) (753 KB) Video obtained at 8 frames/second using SFCM. Field of view: 140 µm x 100 µm. Inset in (a) demonstrates relative field of view of (b); however, it does not necessarily represent the specific image region of (b). Scale bars: 50 µm.

Figure 7 shows a video obtained with the SFCM of the epithelium of oral porcine tissue after application of vinegar for contrast enhancement of nuclei. Cell outlines and nuclei can be visualized, demonstrating the capability of the SFCM to resolve subcellular structure within an intact squamous epithelium. The thickness of the excised tissue is approximately 5 mm; however, penetration depth is limited to approximately 250 µm.

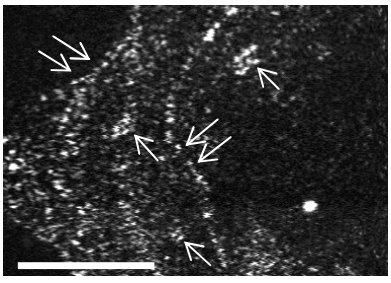

Fig. 7. (707 KB) SFCM video obtained at 8 frames/second of oral porcine tissue after application of vinegar. Single arrows identify nuclei, double arrows identify cell borders. Scale bar: 50 µm.

#72437 - $15.00 USD Received 28 June 2006; revised 30 August 2006; accepted 31 August 2006

4. Discussion

Thus far, the most significant challenge of imaging with the SFCM set-up presented here is limited signal level and penetration depth. This is mainly a result of low reflectivity of the silicon mirror and low reflectance of the tissue samples. The current scanning mirror used to obtain these images is uncoated with an estimated reflectivity of 34%, resulting in significant loss of light in the double pass of the mirror. This can be alleviated by coating future mirrors with a more reflective material, such as gold or aluminum. Our future research plans also include the use of molecular specific gold nanoparticle contrast agents for increased reflectivity from tissue samples. Gold nanoparticles ranging in diameter from 40-80 nm have been demonstrated to have high scattering cross sections for wavelengths in the visible range.

Increased field of view is another significant challenge. Resolution could be compromised to increase field of view, depending on the imaging application; however, this is not a possibility for imaging of cellular structure in tissue. The MEMS device used in the SFCM has two electrodes for each axis. When driving the mirror in resonance, only one electrode is used to swing the mirror through its full range. However, when driving below resonance, which we use for the outer axis for the vertical frame scan, using one electrode produces a scan within half the range. The field of view could be doubled in the vertical direction if appropriate waveforms are applied to the two electrodes of that scan direction. Clearly, the synchronized generation of these two waveforms is more complicated than driving one electrode with a sawtooth waveform. We plan to add this extra scan range in the near future to increase our vertical field of view.

The current set up used to obtain the images in this paper is a bulk-optics demonstration of the potential imaging capability of a miniature confocal microscope. Miniaturization of the optics and repackaging of the MEMS microscanner to enable *in vivo* imaging is currently in progress. A miniature lens system will be designed and constructed to replace the optics located between the microscanner and sample, which are currently the system size-limiting elements. Similar miniature microscopes have been constructed using both glass and plastic complex lens systems [29, 30]. The fiber collimator, MEMS scanner, and compact lens system will be packaged in a probe module for imaging at a fixed depth. Axial scanning could be implemented using translation of an optical window placed between the last lens and the tissue sample using a piezoelectric transducer or hydraulic suction.

5. Conclusion

In conclusion, we have designed and constructed a benchtop prototype of a single fiber confocal microscope using a MEMS two-axis scanner. The imaging system has been characterized, and videos and images have been obtained of cells and tissue. With improvements in mirror reflectivity and miniaturization of optics, a miniature single fiber confocal microscope will have the potential to be used for high resolution *in vivo* imaging.

Acknowledgments

Financial support from the National Institutes of Health is gratefully acknowledged (grants R01 CA82880 and R01 CA103830). This work was also supported by a Korea Research Foundation Grant funded by the Korean Government (MOEHRD, Basic Research Promotion Fund) (KRF-2005-214-C00058).

#72437 - $15.00 USD Received 28 June 2006; revised 30 August 2006; accepted 31 August 2006